1-2015

Validation of volumetric and single-slice MRI adipose analysis using a novel fully automated segmentation method.

Bryan T Addeman

Shelby Kutty

Thomas G Perkins

Abraam S Soliman
Western University, asoliman@uwo.ca

Curtis N Wiens

See next page for additional authors

Authors
Bryan T Addeman, Shelby Kutty, Thomas G Perkins, Abraam S Soliman, Curtis N Wiens, Colin M McCurdy, Melanie D Beaton, Robert A Hegele, and Charles McKenzie

Original Research

Validation of Volumetric and Single-Slice MRI Adipose Analysis Using a Novel Fully Automated Segmentation Method

Bryan T. Addeman, BSc,[1] Shelby Kutty, MD,[2,3] Thomas G. Perkins, PhD,[2,4] Abraam S. Soliman, MSc,[5] Curtis N. Wiens, MSc,[6] Colin M. McCurdy, BSc,[1] Melanie D. Beaton, MD,[7] Robert A. Hegele, MD,[8] and Charles A. McKenzie, PhD[1,5,6,8]*

Purpose: To validate a fully automated adipose segmentation method with magnetic resonance imaging (MRI) fat fraction abdominal imaging. We hypothesized that this method is suitable for segmentation of subcutaneous adipose tissue (SAT) and intra-abdominal adipose tissue (IAAT) in a wide population range, easy to use, works with a variety of hardware setups, and is highly repeatable.

Materials and Methods: Analysis was performed comparing precision and analysis time of manual and automated segmentation of single-slice imaging, and volumetric imaging (78–88 slices). Volumetric and single-slice data were acquired in a variety of cohorts (body mass index [BMI] 15.6–41.76) including healthy adult volunteers, adolescent volunteers, and subjects with nonalcoholic fatty liver disease and lipodystrophies. A subset of healthy volunteers was analyzed for repeatability in the measurements.

Results: The fully automated segmentation was found to have excellent agreement with manual segmentation with no substantial bias across all study cohorts. Repeatability tests showed a mean coefficient of variation of $1.2 \pm 0.6\%$ for SAT, and $2.7 \pm 2.2\%$ for IAAT. Analysis with automated segmentation was rapid, requiring 2 seconds per slice compared with 8 minutes per slice with manual segmentation.

Conclusion: We demonstrate the ability to accurately and rapidly segment regional adipose tissue using fat fraction maps across a wide population range, with varying hardware setups and acquisition methods.

Key Words: abdominal fat; intra-abdominal fat; image processing; subcutaneous fat; visceral adipose tissue; software

J. Magn. Reson. Imaging 2015;41:233–241.

ALONG WITH THE PREVALENCE OF OBESITY, the clinical demand to measure and track adipose tissue distribution increases (1). Adipose tissue has long been regarded as a storage reservoir for triglycerides; however, recent studies suggest that intra-abdominal adipose tissue (IAAT) depots play a more active role in metabolism, impacting a wide variety of clinical risk factors including fasting glucose levels, serum triglycerides, and cholesterol (2,3). IAAT is further associated with type 2 diabetes, cardiovascular disease, hepatic steatosis, hypertension, hyperlipidemia, and all-cause mortality (4–6), escalating the need to quantify regional distribution rather than total adipose tissue.

Adipose quantification using magnetic resonance imaging (MRI) and computed tomography (CT) are accurate and effective measurement methods for fat distribution (7,8). In abdominal fat imaging, acquiring images of the entire visceral cavity without respiratory motion remains a concern for both CT and MRI due to radiation dose (CT), or long scan durations (MRI). As a result, many current clinical quantification techniques use a single transverse slice located at the L2–L5 vertebrae region for use with manual segmentation, as adipose tissue distribution in that slice correlates with total IAAT (9–13). However, single-slice sampling strategies fail when predicting large variations in individual internal fat content (14) and weight loss (15).

[1]Department of Medical Biophysics, University of Western Ontario, London, Ontario, Canada.
[2]University of Nebraska Medical Center, Omaha, Nebraska, USA.
[3]Children's Hospital & Medical Center, Omaha, Nebraska, USA.
[4]Philips Healthcare, Cleveland, Ohio, USA.
[5]Biomedical Engineering, University of Western Ontario, London, Ontario, Canada.
[6]Department of Physics and Astronomy, University of Western Ontario, London, Ontario, Canada.
[7]Department of Medicine, Division of Gastroenterology, University of Western Ontario, London, Ontario, Canada.
[8]Robarts Research Institute, University of Western Ontario, London, Ontario, Canada.

Contract grant sponsor: C.A. McKenzie holds the Canada Research Chair in Translational Magnetic Resonance Imaging at the University of Western Ontario. This research was undertaken, in part, thanks to funding from the Canada Research Chairs Program, NSERC, and the Children's Hospital and Medical Center Foundation Grant.

*Address reprint requests to: C.A.M., University of Western Ontario, Dept. of Medical Biophysics, Natural Science Room 9, 1151 Richmond St., London, Ontario, Canada N6A 5B7.
E-mail: cmcken@uwo.ca

Received July 30, 2013; Accepted November 7, 2013.
DOI 10.1002/jmri.24526
View this article online at wileyonlinelibrary.com.

Table 1
Validation Cohort Details

Validation cohort	*n*	Gender	Age (years) mean [range]	BMI (kg/m^2) mean [range]
Healthy volunteers	8	5 Male/3 Female	31 [24–45]	24.6 [22.3–28.1]
NAFLD	16	9 Male/7 Female	49 [27–72]	31.6 [23.0–41.8]
FPLD2	4	4 Female	38 [32–51]	24.2 [20.3–27.6]
Adolescent	8	4 Male/4 Female	11 [7–19]	22.8 [15.6–31.5]

NAFLD: nonalocholic fatty liver disease; FPLD2: Dunnigan-type familial partial lipodystrophy.

For accurate determination of an individual's IAAT, and intersubject comparison, only multislice imaging will give precise results (16).

Multislice studies which aim to quantify the entire visceral cavity can produce >100 slices per subject, creating large amounts of data for analysis. Manual and semiautomated segmentation can take 3–30 minutes per slice for a trained observer (17), making the use of automated or more efficient semiautomated segmentation essential for volumetric analysis.

With careful selection of image acquisition parameters in techniques such as IDEAL-IQ (18), LAVA-Flex (19), and multipoint Dixon (20) imaging a 3D fat fraction ratio map (fat/[fat+water]) can be measured representing voxel-by-voxel fat fraction values ranging from 0–100% fat (21). Adipose tissue is composed of ~85% fat, 13% water, and 2% proteins (22) and can therefore be differentiated from other lipid-containing tissues in vivo by its high fat fraction values (23). Fat fraction values thus provide a reproducible measure of adipose tissue that does not suffer from relative intensity scales or inhomogeneous image intensities that are inherent with MRI, and can therefore be used for automated quantification with a variety of hardware setups.

Furthermore, water–fat MRI techniques can be combined with accelerated imaging techniques such as parallel MRI (24–26) to rapidly acquire large image volumes. Time constraints become most apparent when performing abdominal imaging where patients are required to hold their breath for the duration of the scan to minimize breathing related artifact. The use of accelerated water–fat imaging techniques allows imaging of the entire visceral cavity from the diaphragm to the pelvic floor within the time of 1 breath-hold (~24 seconds).

Here we propose a novel software package named AdipoQuant for the automated quantification of total adipose tissue (TAT), SAT, and IAAT in the abdomen. The main objective was to develop an automated segmentation method that works with a variety of body types and abnormal fat distributions and assess its precision, accuracy, and repeatability.

MATERIALS AND METHODS

Subjects

Following institutional human studies research ethics board approval and obtaining informed consent, in vivo data were obtained from 36 subjects: 8 healthy volunteers, 16 with nonalcoholic fatty liver disease (NAFLD), 4 with Dunnigan-type familial partial lipodystrophy (FPLD2), and 8 adolescent subjects. Subject statistics are shown in Table 1. NAFLD subjects are significant for automated segmentation, as the exclusion of ectopic fat is required, while FPLD2 subjects have wildly varying fat composition with some having nearly nonexistent subcutaneous fat.

MRI Acquisition

Table 2 describes the MR acquisition details used for each validation cohort.

Healthy Adult MRI Acquisition

Entire visceral cavity scans were acquired during this study with the following parameters. Transverse slices were collected extending from the dome of the liver to the tip of the femoral heads using an investigational version of a parallel MRI accelerated IDEAL sequence on a GE 3.0 T MR750 (GE Healthcare, Waukesha, WI) and a 32-coil torso array (Neo Coil, Pewaukee, WI). The subject's arms were placed at their side and separated from the torso using a foam pad to ensure that the arms were accurately excluded from the abdominal segmentation.

A single acquisition with this investigational version of IDEAL results in the creation of four image series: T2* corrected fat-only, T2* corrected water-only, fat fraction map, and R2* map ([1/T2*]).

FPLD and NAFLD Adult MRI Acquisition

Four FPLD2 and 16 NAFLD datasets available from prior studies were acquired using the following general scan parameters. Transverse images were collected at the L4 vertebra, mid-pelvis, mid-thigh, and mid-calf using an investigational version of the IDEAL sequence (Table 1). Data were acquired with a variety of receive coils (body coil, 8-coil array, and 32-coil array) on a GE 3.0 T MR750 (GE Healthcare).

Adolescent MRI Acquisition

Eight adolescent volunteers were imaged using a 1.5T MRI system (Achieva; Philips Healthcare, Best, The Netherlands). The abdomen was imaged from below the femoral head to above the diaphragm. Two MR image datasets were acquired using a basic breath-hold axial 3D mDIXON protocol (23 sec) and a volunteer-matched field of view (FOV) in the RL and

Table 2
Magnetic Resonance Imaging Acquisition Details

Validation cohort	Acquisition sequence	Field strength (T)	MRI type	Resolution [x,y](mm)	Slice thickness (mm)	Image volume [x,y,z](cm)	Acquisition time(s)
Healthy volunteers (full visceral volume)	IDEAL-IQ	3	GE MR750	[3.2, 3.2]	3.0–5.0	[48, 32, 36]	24–26
NAFLD/FPLD2/healthy volunteers (single-slice)	IDEAL-IQ	3	GE MR750	[2.1, 2.6]	4.0–10.0	[48, 38, 22]	20
Adolescent	mDixon	1.5	Philips Achieva	[3.2, 3.2]	4.0	[48, 34, 40]	17–23

The parameters above were varied among different validation cohorts. In addition, all image acquisitions used an elliptical k-space shutter and a parallel MRI acceleration factor of 3.3.

AP directions to minimize the breath-hold time (17 sec or greater). Fat, water, in-phase, and opposed phase images were reconstructed for each dataset.

Automated Segmentation Method

Step 1: Body Volume Mask

The first objective was to identify a rough mask of the total fat and water tissue volume. This required separation of fat and water tissue from background noise and MR signal voids within the body in areas such as the lungs, bowels, and bone. First, the fat-only and water-only images were added together creating images where fat and water containing tissue such as adipose, organs, and muscles appeared bright (Fig. 1A). An adaptive k-means clustering algorithm was implemented which clustered pixel intensities into three classes: low, medium, and high intensity (Fig. 1B). Then the lowest intensity class was discarded as noise (air- and bone-filled regions), while the medium and high intensity classes were then converted to a binary tissue volume mask (Fig. 1C). A hole filling algorithm was used to fill small voids in the tissue volume mask.

Step 2: Total Adipose Tissue Mask

The tissue volume mask was then applied to the fat fraction map (Fig. 2A) in order to remove nontissue noise voxels. Voxels within the tissue volume mask with fat fraction values higher than 70% fat were located using a simple threshold (Fig. 2B). This high fat fraction threshold avoided including lipid-rich tissues such as bone marrow or steatotic liver. In some subjects, these tissues may have elevated fat fractions up to 50–60%, which would still be excluded by the 70% fat fraction threshold. The threshold resulted in a fat mask containing only adipose tissue, but excluded low fat fraction boundary voxels of adipose tissue which had partial amounts of adipose and water–tissue imaged in the same voxel. This exclusion of boundary adipose tissue due to low fat fraction value is known as partial volume error (PVE). To account for PVE, regions connected to the 70% adipose mask with greater than 40% fat fraction were recovered. The adipose threshold and PVE correction were combined to create the total adipose tissue (TAT) mask (Fig. 2B). In subjects where a R2* map (Fig. 2C) was available, bone marrow and bowels were removed by recognizing areas with much higher R2* values than the muscle, organs and adipose tissue. Figure 2C shows this exclusion.

Step 3: Segmentation of Adipose Tissue Regions

Similar to locating adipose tissue, muscle and organ tissue were found by locating voxels in the volume mask below 50% fat fraction (Fig. 3A). The resulting water mask represented only water tissue proximal to the SAT; the distal edge serves as a general boundary

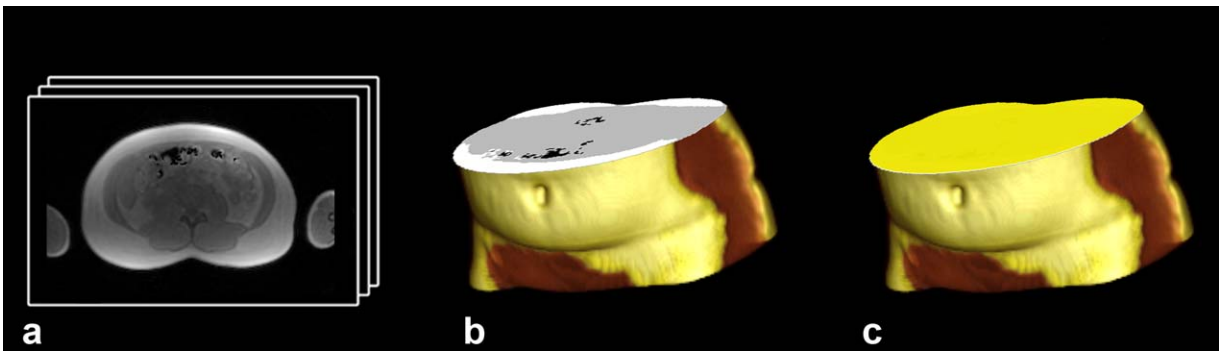

Figure 1. Tissue volume masking illustrates the first step in the segmentation process, segmenting tissue from background noise. (**A**) The in-phase fat+water source image stack is segmented into (**B**) low, medium, and high-intensity classes using a Kmeans clustering algorithm. The lowest signal intensity class is discarded as air/noise and holes are filled in the remaining images to create a (**C**) binary tissue volume mask (solid). [Color figure can be viewed in the online issue, which is available at wileyonlinelibrary.com.]

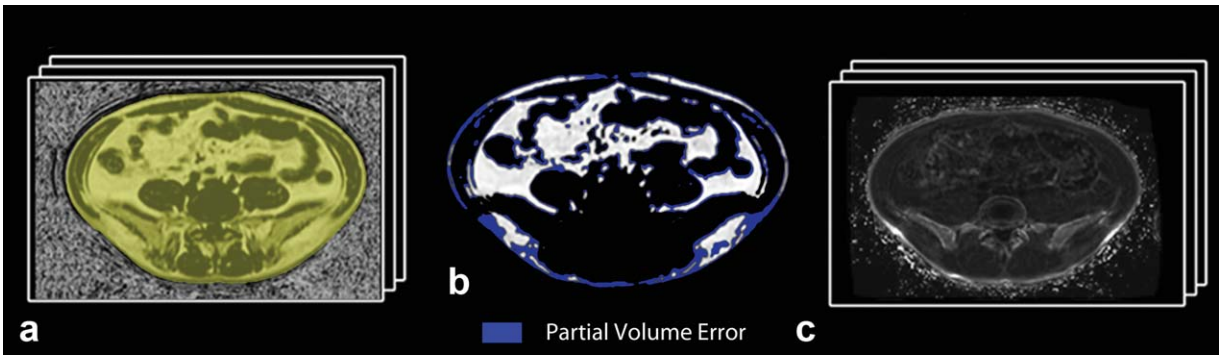

Figure 2. Adipose tissue identification process. The tissue volume mask (yellow) located in Fig. 1 is now applied to the fat fraction images (**A**), masking out the noise. A hard threshold removing all fat fractions below 70% fat is then applied (**B**). To account for PVEs, regions connected to the 70% adipose mask with greater than 40% fat fraction were recovered (blue) using boundary dilation. In subjects where a R2* map (**C**) was available, bone marrow and bowels were removed by recognizing areas with much higher R2* values than the muscle, organs, and adipose tissue.

of the peritoneum. The water mask was converted into polar coordinates such that the distal edge of the tissue appears along the bottom of the image (Fig. 3B). A 3D surface was then fitted to the distalmost edge of each slice's polar water with caution to constrain the smoothness such that areas without water tissue directly adjacent to the SAT were bridged. This surface was then converted back into Cartesian coordinates and enclosed, which resulted in a mask of the intra-abdominal cavity. This mask was then used to split the TAT into SAT and IAAT (Fig. 3C).

Step 4: Calculation of Adipose Tissue Volumes and Tissue Visualization

Adipose volumes were calculated by summing the fat fraction values from each voxel included in the segmented SAT and IAAT. These values were then converted into volumes using a voxel-to-volume conversion factor defined by the acquisition parameters.

Lastly, 3D tissue visualizations of the SAT, IAAT, and water tissue were created (Fig. 4). Each tissue component was rendered separately and was available for viewing as a movable 3D model showing a combination of tissues, or each segmented volume separately.

Method Comparison

For comparison with automated segmentation results, manual segmentation was performed on T2*-corrected fat-only images by a trained observer (B.T.A.) using a previously validated manual segmentation approach (27) designed to quantify and segment subcutaneous and intra-abdominal adipose tissue. The manual segmentation approach works as follows. First, a single fat-only image is loaded into ImageJ (NIH, Bethesda, MD). The observer selects a point on the SAT and uses this as the seed point for the "Connected Threshold Grower" plug-in. The user then defines a lower and upper intensity threshold for adipose tissue based on observation of the image. These threshold values may be altered multiple times by the user to get the desired results. The connected threshold grower then identifies all pixels that are connected to the seed point and have intensity values within the threshold range. Unconnected regions must be connected manually by drawing a thin line on the image between adjacent regions. This is an

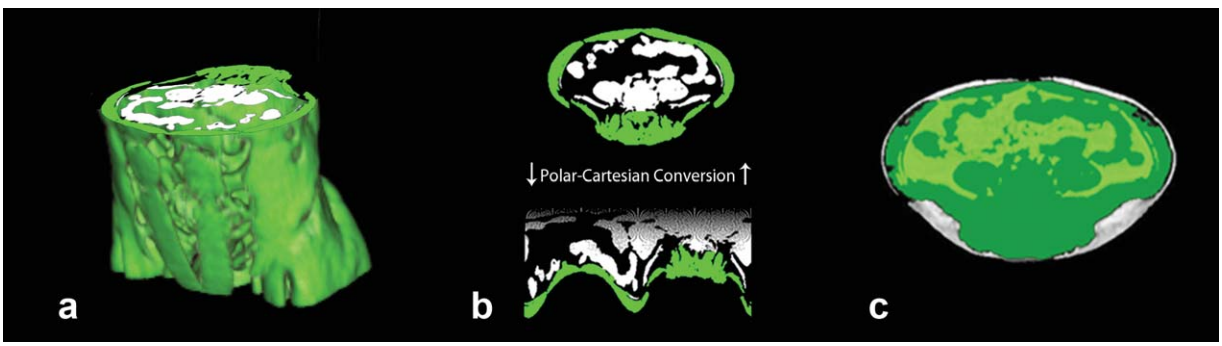

Figure 3. Segmentation of subcutaneous from intra-abdominal adipose tissue. The distal boundaries of the abdominal and back muscles highlighted in green are recognized in this automated method as the boundary between intra-abdominal and subcutaneous adipose tissue. This outer boundary is located by converting the water mask (**A**) into polar coordinates (**B**) such that the distalmost muscle boundary (green) appears along the bottom of the image and can be more easily segmented. A surface is fit over this boundary for each slice, converted back into Cartesian coordinates, and applied to the adipose tissue mask (**C**). Adipose tissue inside this boundary is labeled as intra-abdominal adipose and outside the boundary is labeled subcutaneous adipose.

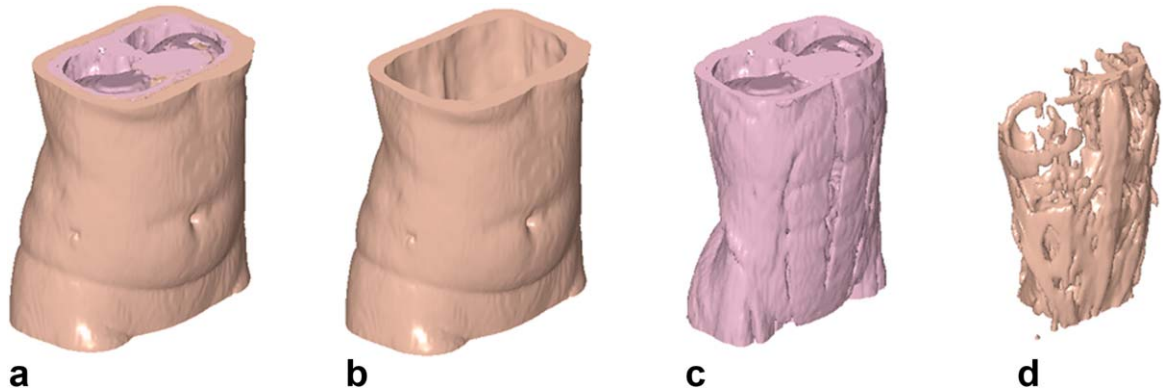

Figure 4. Automated abdominal segmentation of a healthy adult female. Volumetric results are shown for the (**A**) combined fat and water tissue, (**B**) subcutaneous adipose, (**C**) water tissue, and (**D**) intra-abdominal adipose. [Color figure can be viewed in the online issue, which is available at wileyonlinelibrary.com.]

iterative process where the user draws the line, and then runs the connected threshold grower again to check for accuracy. The result is a binary mask of the TAT. The user then disconnects the SAT from IAAT by manually drawing segmentation lines on the image where SAT and IAAT are adjoined.

The processing time per slice for both automated and manual segmentation methods was measured. Since the automated method works on volumetric data, the total processing time was divided by the number of slices in the dataset.

Repeatability and Reproducibility

Four healthy adult volunteers (four male, mean BMI 25.9 ± 2.5, range 22.4–28.1) were each imaged twice on Day 1 and twice on Day 7 in order to assess repeatability and reproducibility of full abdominal SAT, IAAT, and TAT measurements with the proposed method. MRI acquisitions covered the entire visceral cavity from the dome of the liver to the pelvic floor using the healthy adult MRI protocol described above. Repeatability was measured from scan–rescan results performed on the same day, while reproducibility compared the average results between Day 1 and Day 7. Between scan–rescan acquisitions the subject was asked to get up from the table and was repositioned in the coil.

Statistical Analysis

For comparison between manual and automated segmentation methods the absolute volume difference (VD_A) was calculated. VD_A was defined as the absolute difference between automated (A) and manual (M) volumes, divided by the manual volume ($VD_A = |A - M|/M$). A VD_A value of zero would indicate no difference between measurements. For single-slice analysis the VD_A represents comparisons of one slice at the L4 region for each subject. Alternatively, the VD_A for volumetric analysis represents the measured SAT, IAAT, and TAT volumes from all slices within the visceral cavity for each subject.

Bland–Altman plots were used to visualize the agreement between the manual and automated methods (28). Data which formed a horizontal straight line at $x = 0$ would indicate perfect agreement. As well, the mean difference line would be at $x = 0$ indicating no under- or overestimation measurement bias.

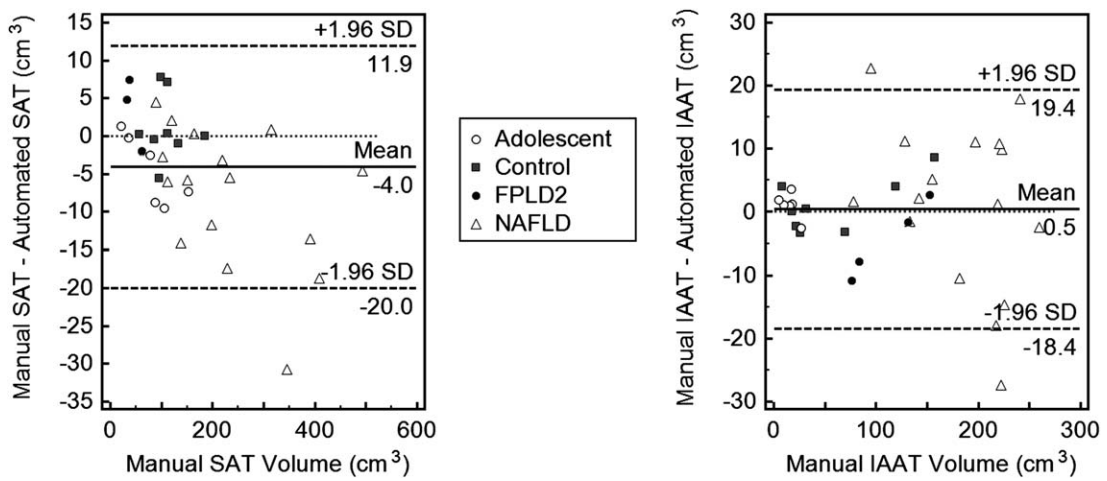

Figure 5. Bland–Altman plot showing the difference between single-slice manual and automated segmentation of SAT and IAAT at the L4 region. Dunnigan-type FPLD2, healthy volunteers (control), NAFLD, and adolescent subjects can be viewed separately. The dashed lines indicate two standard deviations away from the mean difference line (solid).

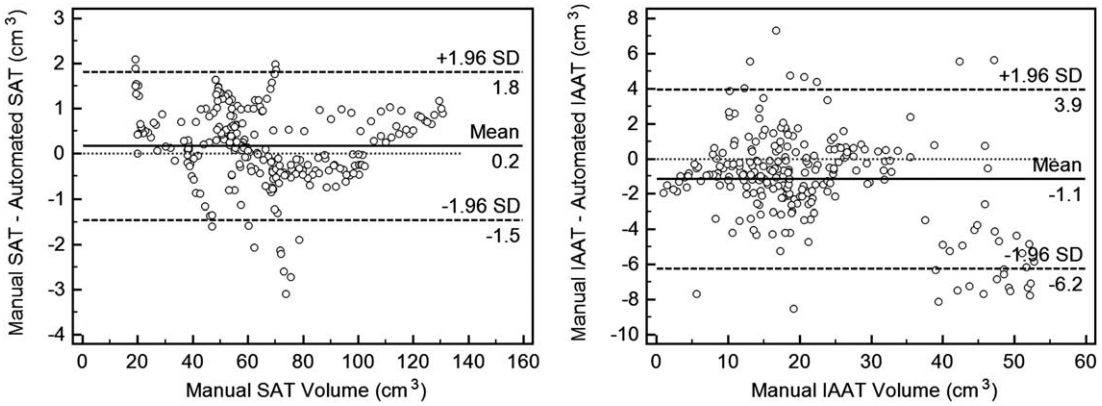

Figure 6. Bland–Altman plot showing the difference between manual and automated segmentation of SAT and IAAT for each slice within the entire 78–88 slice volume of three healthy volunteers. The dashed lines indicate two standard deviations away from the mean difference line (solid).

Comparisons of repeatability and reproducibility were both assessed using the coefficient of variation (CV) metric. CV is defined as the ratio of the standard deviation of the absolute volume differences (σ), to the mean volume measured (μ) with automated segmentation between acquisitions: $CV = \sigma/\mu$.

RESULTS

Two subject datasets from the adolescent subjects were discarded due to excessive motion artifact caused by difficulty in following breath-hold instructions. Otherwise, automated segmentation was successful with all other subjects. Automated analysis required processing time of 2 seconds per slice using the AdipoQuant software on a Mac Pro (2.4 GHz, 8 GB RAM). Manual analysis required 8 minutes per slice. Each volume (78–88 slices) was completed within 2 minutes, while manual segmentation required at least 6 hours.

For single-slice analysis at the level of the L4 vertebra, the mean VD_A was 6.2 ± 6.6 cm^3 ($4.7 \pm 4.5\%$) for SAT, and 6.7 ± 6.8 cm^3 ($9.0 \pm 10.2\%$) for IAAT. The Pearson correlations were ($R^2 = 0.997$), and ($R^2 = 0.987$) for SAT, and IAAT. Bland–Altman plots show that the two methods had good agreement with no substantial bias (Fig. 5).

For volumetric analysis, the mean VD_A was 39.8 ± 28.44 cm^3 ($1.1 \pm 0.7\%$) for SAT, and 93.1 ± 80.9 cm^3 ($5.0 \pm 3.3\%$) for IAAT. The Pearson correlations were ($R^2 = 0.999$), and ($R^2 = 0.967$) for SAT and IAAT, respectively. Result comparisons for each slice within the volume are summarized in Fig. 6, indicating the accuracy for each anatomical location within the abdominal volume.

Data from the repeatability and reproducibility acquisitions also showed excellent agreement and were nearly identical in values. The coefficients of variation for scan–rescan repeatability measurements were $1.2 \pm 0.6\%$ for SAT and $2.7 \pm 2.2\%$ for IAAT. For reproducibility data acquired on Day 1 and Day 7, the coefficients of variation were $1.8 \pm 2.6\%$ for SAT, and $3.0 \pm 2.1\%$ for IAAT.

Table 3 summarizes our algorithm compared with recent publications of alternative volumetric analysis segmentation approaches by Wald et al (29), and Thormer et al (30).

DISCUSSION

We have demonstrated the ability to automatically segment regional adipose tissue with a high degree of accuracy and repeatability. This includes a variety of subjects (lean, obese, adolescent, and rare fat

Table 3
Volumetric Analysis Literature Comparison

	Segmentation process comparison		Results comparison		
Author	Adipose identification	SAT/IAAT segmentation	Processing time (s)	Mean VD_A (%, cm^3)	Repeatability (CV%)
Addeman et al	Fat fraction threshold, PVE correction	Polar conversion, surface fitting	2	SAT: 0.9%, 39.8 cm^3 IAAT: 5.0%, 93.1 cm^3	SAT: 1.2% IAAT: 2.7%
Wald et al (29)	Histogram threshold	Statistical shape modeling	0.5	SAT: 0.9%, 48.64 cm^3 IAAT: 4.2%, 143.8 cm^3	SAT: 0.35% IAAT: 3.50%
Thormer et al (30)	Histogram threshold	Snake algorithms	19	SAT: 4.7%*, 663 cm^{3*} IAAT: 6.3%*, 343 cm^{3*}	N/A

Mean VD_A, The mean absolute volume difference between automated and manual segmentation methods; CV, coefficient of variation; Processing Time, processing timer per slice; *estimated from values on Bland-Altman plot.

Table 4
Clinical Implication: Measured Adipose Volumes

Validation cohort	TAT (cm^3)	SAT (cm^3)	IAAT (cm^3)	IAAT/SAT ratio
Healthy volunteers	164.4	108.8	55.5	0.51
Adolescent	100.3	85.5	14.7	0.17
NAFLD	421.9	239.6	152.3	0.64
FPLD2	161.4	46.2	115.2	2.49

TAT, total adipose tissue (SAT+IAAT); SAT, subcutaneous adipose tissue; IAAT, intra-abdominal adipose tissue.

distribution cohorts) as well as imaging strategies and platforms (IDEAL-IQ using a 3T GE MR750 and mDixon using a 1.5T Philips Achieva). The results were very similar to those obtained by standard manual segmentation methods, but required no manual intervention and could be calculated very rapidly over complete image volumes.

Data from NAFLD and FPLD2 patients were retrospective and not acquired with full abdominal volumetric coverage. As a result, single-slice analysis was used to assess the accuracy of the automated algorithm in varying study cohorts. In addition, due to the labor-intensive manual segmentation requiring more than 6 hours per volume, volumetric manual segmentation was not feasible for all patients.

Ultimately, the goal of any segmentation algorithm is to extract the clinical implications measured through imaging. The mean measured SAT and IAAT volumes are compared for each validation cohort (Table 4), and even with relatively small validation cohorts there are noticeable differences between the IAAT to SAT ratios of the cohorts. This is most apparent when comparing the lipodystrophy (FPLD2) and healthy adult volunteer cohorts. Both have similar amounts of total adipose tissue, but FPLD2 subjects store a far larger proportion of fat in the IAAT compartment, resulting in a higher clinical risk of experiencing metabolic related disorders.

Relative image intensity scale, the inhomogeneous image intensity of MRI, and large differences in abdominal size and shape between subjects traditionally make accurate analysis of adipose tissue volume difficult (1). Techniques where signal intensities vary more drastically with radial distance from the coil further complicates the problem. For example, parallel MRI uses multicoil arrays for improved image quality and reduced scan times at the price of significant signal intensity variation. Automated techniques that use histogram thresholds to segment adipose based on signal intensity have been developed (31–33). However, the prevalence of signal intensity variations in MRI and parallel MRI make histogram threshold techniques inherently unreliable. This is due to variation in signal intensities of the same tissue not only between test facilities, but also between acquisitions in the same facility.

Prior knowledge approaches that attempt to model the shape of adipose structures are often used in automated segmentation as well, limiting the technique to use with smaller ranges of body types and fat distributions. Thus, many segmentation techniques have been developed for use with obese patients, likely due to the fact that lean subjects are historically more difficult to automatically segment than subjects with greater amounts of adipose tissue (34,35). The method introduced in this study takes an alternative approach and segments the adipose tissue based on its position relative to the muscle tissue. As a result, lean patients can also be automatically segmented effectively since the most superficial muscle tissue can be easily delineated by its high water content. The proposed algorithm was suitable for use with all body types without the need for calibration between subjects.

Reproducibility between test centers and acquisition hardware is important for the mainstream use of any MRI-based automated adipose segmentation. Proton density fat fraction (PDFF) images, such as those created in IDEAL, are recognized as a biomarker which can be accurately reproduced regardless of acquisition hardware setup (21). In contrast, T1-weighted images are often used for adipose tissue analysis and are less robust to hardware changes. Additionally, T1 imaging can cause difficulty in segmentation due to an overlap in signal intensity from the liver and adipose tissue, causing ambiguity in accurate segmentation (14,36,37). Using IDEAL for fat segmentation is superior to T1-weighted imaging because of the unambiguous identification of fat by IDEAL (38). Importantly, our results demonstrate the ability to successfully segment fat fraction images collected from three separate test facilities using varying acquisition methods and hardware.

The time required for automated segmentation using our method provides a large advantage over manual segmentation and other semiautomated and fully automated software packages available. Manual, semiautomated, and even fully automated segmentation have been reported to take anywhere from 3–30 minutes per slice by a trained observer (17). With our automated method, the time required for segmentation is 1–2 seconds per slice and does not require a trained observer. This reduction in analysis time makes it feasible to measure the adipose distribution of the entire visceral cavity and other large volumes at high resolutions.

For accurate adipose tissue segmentation, two possible sources of error must be addressed. First, the ambiguity of voxels filled with partial volumes of boundary adipose tissue can result in a significant source of error if not accounted for (39). Since partial volume voxels have similar signal intensities or fat fractions as other nonadipose fat structures such as bone marrow and ectopic fat, it has traditionally been difficult to automatically identify. In fat fraction images, the partial volume voxels can be recognized by their fat fraction values in combination with their location; they will always be located adjacent to connected regions of full adipose volume voxels. Second, additional exclusions of bowel contents, intramuscular fat, spine and vertebrae, blood vessels, and other nonrelevant structures are required since they can have signal intensities that mimic fat (40). Many of these structures can be excluded using a combination

of the fat fraction map, fat and water images, and the R2* map. For instance, ectopic fat found in the liver of NAFLD patients is often in the 10–25% fat range, increasing to >50% in rare cases. These areas fall far below the adipose tissue fat fraction threshold of 70% fat. As well, they do not fit the criteria of PVE voxels as they are not directly connected to full volume adipose voxels, with the exception of some organ boundaries. This method is also used to remove intramuscular fat and most bone marrow. An advantage of using the IDEAL acquisition method where R2* maps are available is that trapped gases and solid structures appear bright in contrast to muscle, organ, and fatty tissue. With the presence of an accurate R2* map we have demonstrated the ability to correct for bowel gas and contents and model the spine and iliac crests.

Comparing the segmentation process with alternate methods (Table 3), our method is unique in using the fat fraction map for adipose tissue identification rather than a histogram threshold on the fat-only images. The challenge with using fat-only images for segmentation, which are measured in relative units, is that the signal intensity used to identify adipose tissue is inherently changing. Depending on the hardware used to collect the images the intensity of adipose tissue can change so drastically that any type of threshold approach will introduce bias in fat measurement related to where the tissue is located within the volume.

Comparing results between algorithms remains difficult since the reference standard method of manual segmentation is calculated slightly different by each group and has its own issues with precision and accuracy. The reported precision, repeatability, and processing time of our proposed method is similar to that of recently published work by Wald et al, which are among the most precise current results for volumetric analysis. Further reduction in the processing time of our algorithm could be achieved by implementation in C++, as is the algorithm of Wald et al. The advantage of our algorithm is that the identification of fat is based on analysis of fat fraction values, which are more stable to changes in hardware, testing site, and imaging methods. Using fat fraction values also allows for more accurate correction of partial volume error, which is especially important in lean subjects and adolescents. Also, to our knowledge the proposed method is the first to introduce the use of R2* maps for automated removal of bone marrow and bowel contents.

Future work is needed to broaden the application for use with cardiac/thoracic imaging, full body scans, and animal models. There is interest in quantifying epicardial adipose tissue for its effect on cardiac function. However, challenges exist in MRI fat fraction acquisition due to cardiac motion. Full-body fat distribution analysis is desirable, but due to long scan times and the inability to cover the entire body in one acquisition, data collection must be done in portions and then stitched together later. As acquisition techniques evolve, our automated segmentation method can be easily adapted to accommodate full-body analysis. Finally, challenges also exist with small animal imaging due to cardiac motion and small imaging volumes. Typically, it has been difficult to get sufficient resolution fat fraction images in mice and rats to delineate the abdominal muscle wall from the subcutaneous adipose, but as hardware has improved we are beginning to acquire suitable images. Preliminary work has been done by our research group and has shown success with automated segmentation of mice and rats.

Acquiring high-resolution, artifact-free images remains a limitation for data collection. Populations like adolescents, the elderly, and the morbidly obese may have difficulties following breath-hold instructions, which creates reliability issues with the image acquisition. Free-breathing protocols are available and should be implemented if possible to reduce the strain on the subject. In addition, fully automated algorithms are always prone to failure on select datasets. The ability for an enduser to correct for errors which may occur during segmentation, or further segment the images, can only add to the value and robustness of any automated analysis tool. These features are part of the proposed segmentation software, but were not used for the purposes of this publication.

In conclusion, we have demonstrated the ability to automatically segment regional adipose tissue using fat fraction maps to accurately quantify TAT, SAT, and IAAT. The results are very similar to those obtained by standard manual segmentation methods, are repeatable, and are calculated very rapidly over complete imaging volumes.

ACKNOWLEDGMENT

The authors thank all volunteers who participated in the study.

REFERENCES

1. Kullberg J, Johansson L, Ahlstrom H, et al. Automated assessment of whole-body adipose tissue depots from continuously moving bed MRI: a feasibility study. J Magn Reson Imaging 2009;30:185–193.
2. Bergman RN, Kim SP, Catalano KJ, et al. Why visceral fat is bad: mechanisms of the metabolic syndrome. Obesity 2006;14(Suppl 1):16S–19S.
3. Weltman A, Despres JP, Clasey JL, et al. Impact of abdominal visceral fat, growth hormone, fitness, and insulin on lipids and lipoproteins in older adults. Metab Clin Exp 2003;52:73–80.
4. Despres JP, Lemieux I. Abdominal obesity and metabolic syndrome. Nature 2006;444:881–887.
5. Kuk JL, Katzmarzyk PT, Nichaman MZ, Church TS, Blair SN, Ross R. Visceral fat is an independent predictor of all-cause mortality in men. Obesity (Silver Spring) 2006;14:336–341.
6. Wajchenberg BL. Subcutaneous and visceral adipose tissue: their relation to the metabolic syndrome. Endocr Rev 2000;21:697–738.
7. Shen W, Liu H, Punyanitya M, Chen J, Heymsfield SB. Pediatric obesity phenotyping by magnetic resonance methods. Curr Opin Clin Nutr Metab Care 2005;8:595–601.
8. Ross R. Advances in the application of imaging methods in applied and clinical physiology. Acta Diabetol 2003;40(Suppl 1):S45–50.
9. Han TS, Kelly IE, Walsh K, Greene RM, Lean ME. Relationship between volumes and areas from single transverse scans of intra-abdominal fat measured by magnetic resonance imaging. Int J Obes Relat Metab Disord 1997;21:1161–1166.

10. Kuk JL, Church TS, Blair SN, Ross R. Does measurement site for visceral and abdominal subcutaneous adipose tissue alter associations with the metabolic syndrome? Diabetes Care 2006;29: 679–684.
11. Shen W, Punyanitya M, Chen J, et al. Visceral adipose tissue: relationships between single slice areas at different locations and obesity-related health risks. Int J Obes 2007;31:763–769.
12. Shen W, Punyanitya M, Wang Z, et al. Visceral adipose tissue: relations between single-slice areas and total volume. Am J Clin Nutr 2004;80:271–278.
13. Abate N, Garg A, Coleman R, Grundy SM, Peshock RM. Prediction of total subcutaneous abdominal, intraperitoneal, and retroperitoneal adipose tissue masses in men by a single axial magnetic resonance imaging slice. Am J Clin Nutr 1997;65:403–408.
14. Thomas EL, Saeed N, Hajnal JV, et al. Magnetic resonance imaging of total body fat. J Appl Physiol 1998;85:1778–1785.
15. Shen W, Chen J, Gantz M, Velasquez G, Punyanitya M, Heymsfield SB. A single MRI slice does not accurately predict visceral and subcutaneous adipose tissue changes during weight loss. Obesity 2012;20:2458–2463.
16. Thomas EL, Bell JD. Influence of undersampling on magnetic resonance imaging measurements of intra-abdominal adipose tissue. Int J Obes Relat Metab Disord 2003;27:211–218.
17. Bonekamp S, Ghosh P, Crawford S, et al. Quantitative comparison and evaluation of software packages for assessment of abdominal adipose tissue distribution by magnetic resonance imaging. Int J Obes (Lond) 2008;32:100–111.
18. Reeder SB, McKenzie C, Pineda AR, et al. Water–fat separation with IDEAL gradient-echo imaging. J Magn Reson Imaging 2007; 25:644–652.
19. Ma J. Dixon techniques for water and fat imaging. J Magn Reson Imaging 2008;28:543–558.
20. Eggers H, Brendel B, Duijndam A, Herigault G. Dual-echo Dixon imaging with flexible choice of echo times. Magn Reson Med 2013;65:96–107.
21. Reeder SB, Hu HH, Sirlin CB. Proton density fat-fraction: a standardized MR-based biomarker of tissue fat concentration. J Magn Reson Imaging 2012;36:1011–1014.
22. Thomas LW. The chemical composition of adipose tissue of man and mice. Q J Exp Physiol Cogn Med Sci 1962;47:179–188.
23. Hu HH, Smith DL Jr, Nayak KS, Goran MI, Nagy TR. Identification of brown adipose tissue in mice with fat-water IDEAL-MRI. J Magn Reson Imaging 2011;31:1195–1202.
24. Griswold MA, Jakob PM, Heidemann RM, et al. Generalized autocalibrating partially parallel acquisitions (GRAPPA). Magn Reson Med 2002;47:1202–1210.
25. Pruessmann KP, Weiger M, Scheidegger MB, Boesiger P. SENSE: sensitivity encoding for fast MRI. Magn Reson Med 1999;42:952–962.
26. Sodickson DK, Manning WJ. Simultaneous acquisition of spatial harmonics (SMASH): fast imaging with radiofrequency coil arrays. Magn Reson Med 1997;38:591–603.
27. Alabousi A, Al-Attar S, Joy TR, Hegele RA, McKenzie CA. Evaluation of adipose tissue volume quantification with IDEAL fat-water separation. J Magn Reson Imaging 2012;34:474–479.
28. Bland JM, Altman DG. Measuring agreement in method comparison studies. Stat Methods Med Res 1999;8:135–160.
29. Wald D, Teucher B, Dinkel J, et al. Automatic quantification of subcutaneous and visceral adipose tissue from whole-body magnetic resonance images suitable for large cohort studies. J Magn Reson Imaging 2012;36:1421–1434.
30. Thormer G, Bertram HH, Garnov N, et al. Software for automated MRI-based quantification of abdominal fat and preliminary evaluation in morbidly obese patients. J Magn Reson Imaging 2013; 37:1144–1150.
31. Kullberg J, Ahlstrom H, Johansson L, Frimmel H. Automated and reproducible segmentation of visceral and subcutaneous adipose tissue from abdominal MRI. Int J Obes (Lond) 2007;31:1806–1817.
32. Liou TH, Chan WP, Pan LC, Lin PW, Chou P, Chen CH. Fully automated large-scale assessment of visceral and subcutaneous abdominal adipose tissue by magnetic resonance imaging. Int J Obes (Lond) 2006;30:844–852.
33. Positano V, Gastaldelli A, Sironi AM, Santarelli MF, Lombardi M, Landini L. An accurate and robust method for unsupervised assessment of abdominal fat by MRI. J Magn Reson Imaging 2004;20:684–689.
34. Elbers JM, Haumann G, Asscheman H, Seidell JC, Gooren LJ. Reproducibility of fat area measurements in young, non-obese subjects by computerized analysis of magnetic resonance images. Int J Obes Relat Metab Disord 1997;21:1121–1129.
35. Staten MA, Totty WG, Kohrt WM. Measurement of fat distribution by magnetic resonance imaging. Invest Radiol 1989;24:345–349.
36. Brennan DD, Whelan PF, Robinson K, et al. Rapid automated measurement of body fat distribution from whole-body MRI. AJR Am J Roentgenol 2005;185:418–423.
37. Kullberg J, Angelhed JE, Lonn L, et al. Whole-body T1 mapping improves the definition of adipose tissue: consequences for automated image analysis. J Magn Reson Imaging 2006;24:394–401.
38. Alabousi A, Al-Attar S, Joy TR, Hegele RA, McKenzie CA. Evaluation of adipose tissue volume quantification with IDEAL fat-water separation. J Magn Reson Imaging 2011;34:474–479.
39. Zhou A, Murillo H, Peng Q. Impact of partial volume effects on visceral adipose tissue quantification using MRI. J Magn Reson Imaging 2011;34:1452–1457.
40. Hu HH, Nayak KS, Goran MI. Assessment of abdominal adipose tissue and organ fat content by magnetic resonance imaging. Obes Rev 2013;12:e504–515.